Applied Surface Science 258 (2012) 4016–4022

Contents lists available at SciVerse ScienceDirect

Applied Surface Science

journal homepage: www.elsevier.com/locate/apsusc

Low-temperature solvothermal synthesis of visible-light-responsive S-doped TiO_2 nanocrystal

Guidong Yang[a,b], Zifeng Yan[b,*], Tiancun Xiao[c,**]

[a] Department of Chemical Engineering, State Key Laboratory of Multiphase Flow in Power Engineering, Xi'an Jiaotong University, Xi'an, 710049, China
[b] State Key Laboratory for Heavy Oil Processing, China University of Petroleum, Qingdao, 266555, China
[c] Department of Chemistry, Inorganic Chemistry Laboratory, University of Oxford, Oxford, OX1 3QR, UK

ARTICLE INFO

Article history:
Received 24 October 2011
Received in revised form
14 December 2011
Accepted 17 December 2011
Available online 26 December 2011

Keywords:
Sulfur
Doping
TiO_2
Visible light
Photocatalysis
Solvothermal

ABSTRACT

In this work, a low-temperature solvothermal method has been developed to synthesize visible-light-responsive S-doped TiO_2 nanocrystal photocatalyst, using thiourea as the sulfur source to enhance sulfur incorporation into TiO_2 lattice. The effects of different S:Ti molar ratio on the crystal structure, chemical composition, surface property and catalytic performance have been studied. X-ray photoelectron spectroscopy (XPS) analysis and Fourier transform infrared (FT-IR) spectra displayed that the TiO_2 was modified by the S element incorporated into the TiO_2 network to form Ti—O—S bond, which therefore led to the formation of intermediate energy level just above the O 2p valance band, and caused the absorption edge of TiO_2 to shift into the visible light region up to 500 nm. Characterization results show that the pure nanocrystal anatase structure, with both the degree of S doping and oxygen vacancies makes contribution to the exceptional photocatalytic activity of TONS in visible-light degradation of Methylene Blue (MB) and phenol molecules.

1. Introduction

In the past decade, photocatalytic degradation of organic pollutants and water splitting by some semiconductors, such as TiO_2 [1], ZnO [2] and SnO_2 [3], have been attracting lots of attention, which is considered as a promising technique to solve the environmental and energy problem [1–5]. Among these photomaterials, titanium dioxide (TiO_2) materials have been extensively studied due to its stability and low cost, in addition to its potential application in solar energy conversion and environmental purification [4–6]. Recently, nanostructured TiO_2 with large surface areas and well anatase crystalline have proved to be excellent candidates for these applications [7], not only due to the novel properties and functions associated with individual nanostructure but also because of the new collective properties and advanced tunable functions arising from nanostructure ensembles [8]. However, the main drawback is that TiO_2 nanoparticles may only be excited by ultraviolet (UV) light (wavelength $\lambda < 388$ nm) owing to their wide band gap. Therefore, the overall efficiency of TiO_2 remains too lower under natural sunlight irradiation, as the UV only accounts for about 4% of the incoming solar energy on the Earth's surface [9]. Nevertheless, a rapid recombination rate of light-excited charges also greatly reduces the quantum efficiency of TiO_2 and further limits its application [10].

In order to enhance photocatalytic activity of TiO_2 and shift its absorption from the UV region into the visible-light region, lots of researches have been carried out in the field of visible-light induced TiO_2 by impurity doping [11], novel metal deposition [12,13] and composite semiconductor [14,15]. Among these, a promising strategy involves low-level doping of TiO_2 with nonmetal such as N [16], F [17] and C [18] has been intensively investigated and used to extend the optical absorption edge of wide band gap semiconductors. Compared to the other nonmetals, doping with sulfur has been much less studied. Thus, in attempt to improve the visible-light photocatalytic performance, various physicochemical methods have been applied to modify TiO_2 photocatalyst doped with S element. Chen and Burda [19] demonstrated that S-doped TiO_2 prepared with a high-temperature oxidation method by oxidizing titanium carbide, exhibits strong absorption in visible light region, due to the nonmetal element doping of TiO_2 leads to an increase of the density of states just above the TiO_2 valence band edge. Li et al. [20] treated the TiO_2 precursor under supercritical conditions with CS_2/ethanol as a fluid to synthesize S-doped TiO_2, it was found that their samples of S-modified TiO_2 showed a red-shifted absorption spectrum and exhibited much higher activity than the undoped TiO_2 in photocatalytic degradation of Methylene Blue (MB).

* Corresponding author. Tel.: +86 532 86981296; fax: +86 532 86981295.
** Corresponding author. Tel.: +44 1865 272660; fax: +44 1865 272690.
E-mail addresses: zfyancat@upc.edu.cn (Z. Yan), Xiao.tiancun@chem.ox.ac.uk (T. Xiao).

0169-4332/$ – see front matter © 2011 Elsevier B.V. All rights reserved.
doi:10.1016/j.apsusc.2011.12.092

Herein, we developed a simple preparation method for the synthesis of S-doped TiO_2 nanomaterial at low temperature whereby an ethanol–water solvothermal method with thiourea as the sulfur source to enhance sulfur incorporation into TiO_2 lattice is used. The prepared TiO_2 materials are characterized by XRD, XPS, Raman spectroscopy, FT-IR, SEM and UV–vis DRS spectrophotometer. The photocatalytic activity of the S-doped TiO_2 photocatalyst was evaluated using the decomposition of Methylene Blue and phenol solution as a model reaction. Characterization results show that the S doping level has a remarkable effect on the crystalline phase, optical absorption, surface composition and catalytic performance of doped TiO_2 samples. The activity of obtained photocatalysts under visible light illumination can be enhanced significantly for photocatalytic degradation of organic pollutants.

2. Experimental

2.1. Catalyst preparation

The S-doped TiO_2 samples were prepared according to the following procedure. Typically, 0.01 mol $Ti(OBu)_4$ was dispersed into 30 ml of absolutely ethanol, while 1 ml of acetic acid was added in the above mixture to form solution A. Under vigorous stirring, the desired amount of thiourea (CH_4H_2S, the molar ratio of S to Ti = 0.5, 1.0 and 1.5) was dissolved into 20 ml of ethanol for 1 h to form suspension B. The two solutions were then mixed for 10 min, and 1 ml of deionized water was added into the mixture with a further 30 min stirring. After that, the resultant slurry was transferred into a Teflon-lined autoclave and heated at 120 °C for 24 h. Then the autoclave was taken out from the oven and cooled to room temperature naturally. The S-doped TiO_2 was collected by centrifugation, washing and then dried at 80 °C overnight prior to annealing at 450 °C for 3 h in air. Finally, the obtained doped catalyst with different S:Ti molar ratios of 0.5, 1.0 and 1.5 were denoted as TONS-0.5, TONS-1.0 and TONS-1.5, respectively. The undoped TiO_2 was prepared by the same approach. The commercial Degussa P25 TiO_2 was used here as a reference without any treatment.

2.2. Material characterization

The crystalline structure and phase component of the TiO_2 samples were determined with X-ray diffraction (XRD) using a Philips X-PeRT Pro Alpha 1 diffractometer operating with Cu Kα radiation (λ = 1.5406 Å) at a tube current of 40 mA and a voltage of 45 kV. Data were collected over 2θ values from 20° to 80° at a speed of 1°/min. The X-ray photoelectron spectroscopy (XPS) measurements were carried out using a PerkinElmer RBD upgraded PHI-5000C ESCA system with monochromatic Mg Kα excitation and a charge neutralizer. All bonding energies were calibrated to the C 1s peak at 284.8 eV of the surface adventitious carbon. Laser Raman spectra were obtained using a PerkinElmer Ramanstation 400F Raman spectrometer. UV–vis diffuse reflectance was recorded in a PerkinElmer Lambda 750S UV–vis spectrometer equipped with an integrated sphere. The geometry and morphology of the S-doped TiO_2 materials were investigated by JSM840F scanning electron microscopy (SEM). Fourier transform infrared (FT-IR) spectra were carried out Bruker Vertex-70 by diffused reflectance accessory technique.

3. Activity test

Photocatalytic reactions were conducted in an open reactor with a cooling-water-cycle system keeping the reaction temperature constant. The light source was a 300 W Xenon lamp (Trusttech, Beijing, China), emitting UV and visible light simultaneously. For visible light measurements, a 420 nm cut-off glass filter was mounted before the output of light source to remove UV light and admit only visible light to enter into the reactor. The synthesized S-doped TiO_2 catalyst (100 mg) was suspended in 100 ml of Methylene Blue and phenol (10 mg L^{-1}) solution, respectively. Before the photoreaction, the suspension was stirred in the dark for 240 min to make sure the mixture had achieved adsorption/desorption equilibrium, then 3 ml of the solution was taken from the reactor in a constant time, the sample powder was separated from the solution by a centrifugation method. The concentration of the remaining transparent liquid was analyzed in a UV–vis spectrophotometer. It should be noted that no sacrificial agent and oxygen were added into the solution during the reaction process.

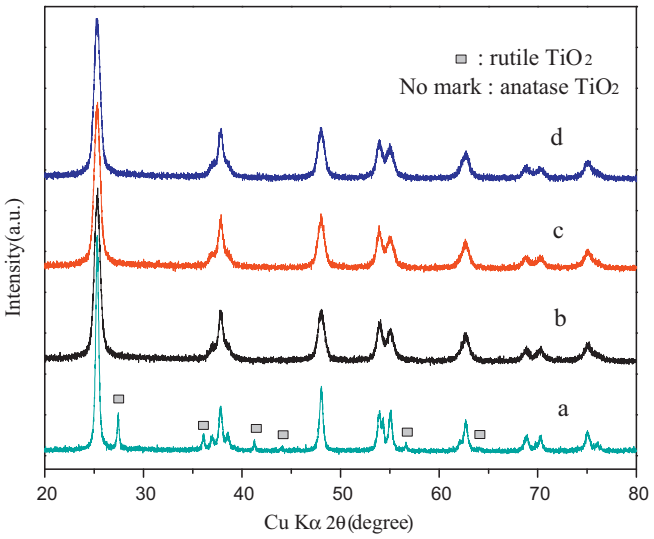

Fig. 1. XRD patterns of S-doped TiO_2 and pure TiO_2 samples, (a) P25 TiO_2, (b) TONS-0.5, (c) TONS-1.0, (d) TONS-1.5. All samples were calcined at 450 °C for 3 h.

4. Results

Fig. 1 shows the X-ray diffraction data of S-doped TiO_2 prepared with different molar ratios of sulfur to titanium, including the undoped commercial TiO_2. Degussa P25 is composed of 75–80% anatase phase and 20–25% rutile phase, with average size of 33 nm, and used here as a reference. All the doped samples showed a unique anatase phase, no other phases such as S containing compounds can be found in the XRD patterns, suggesting that no impurity species were formed during the doping process. The main Bragg diffractions of S-doped TiO_2 is observed to become sharp with the increase of the S doping level, indicating that TONS series sample have highly crystallinity. The average particle size of S-doped anatase TiO_2, estimated by Scherrer equation were listed in Table 1. It can be seen that the grain sizes of TONS-0.5, TONS-1.0 and TONS-1.5 samples are determined as 11.8, 11.1 and 11.4 nm, respectively, which are much smaller than that of undoped TiO_2. This observation displayed that S doping could efficiently restrict the growth

Table 1
Crystal size and phase composition of S-doped TiO_2 with different starting S:TiO_2 molar ratios.

Sample	S/TiO_2 molar ratio	Phase composition	Average crystallite size (nm)
TONS-0.5	1/2	Anatase	11.8
TONS-1.0	1/1	Anatase	11.1
TONS-1.5	3/2	Anatase	11.4
P25 (reference)	–	Anatase, rutile	33.0

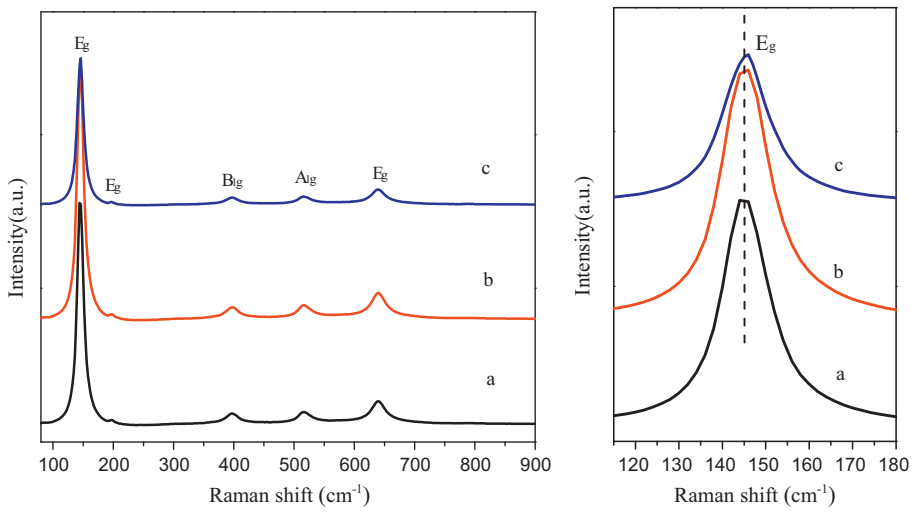

Fig. 2. Laser Raman spectra of S-doped TiO_2 with different doping level and the inset shows the expanded views of E_g Raman band. (a) TONS-0.5, (b) TONS-1.0, (c) TONS-1.5.

of grain size owing to the incorporation of the S dopant into TiO_2 lattice.

The phase evolution of the oxides prepared in this work was also investigated using Raman spectroscopy. As shown in Fig. 2, the Raman spectrum of doped TiO_2 exhibits five bands at 143 cm^{-1} (E_g), 197 cm^{-1} (E_g), 399 cm^{-1} (B_{1g}), 514 cm^{-1} (A_{1g}) and 639 cm^{-1} (E_g). All the bands could be attributed to Raman resonances anatase phase [21,22], with no peaks arising from the rutile phase. In addition, S doping did not cause the appearance of any additional bands, and these results are consistent with the XRD analysis. It was reported that the Raman scattering can be used to estimate the crystallize size of doped TiO_2 [23,24]. The inset of Fig. 2 shows the expanded views of E_g Raman band. It was found that increasing S doping had a little effect on the frequencies of the fundamental

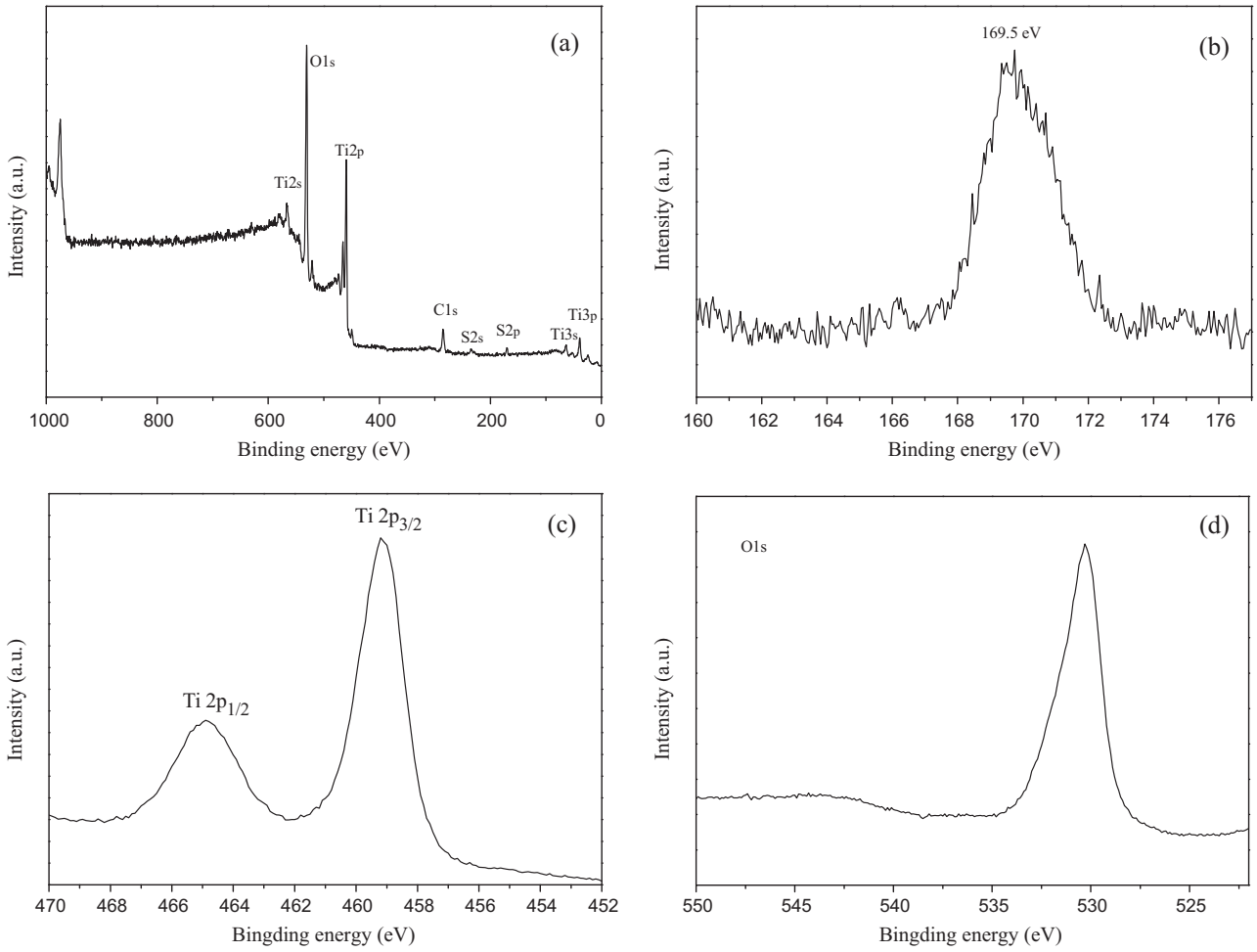

Fig. 3. The XPS spectra of TONS-1.0 sample (a) the survey spectra of S-doped TiO_2, (b) S 2p XPS spectra, (c) Ti 2p XPS spectra, (d) O 1s XPS spectra.

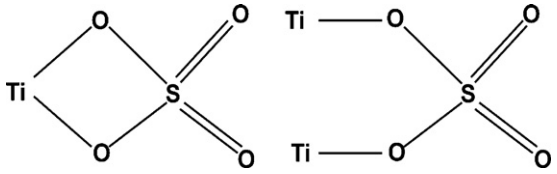

Fig. 4. Coordination models between SO_4^{2-} and TiO_2.

vibrations, and that the E_g band at 143 cm^{-1} in bulk anatase shifts to higher wavenumber with increasing S doping. This suggests that the particle size of doped samples decreases with increasing S doping, and also confirms that the oxides are obtained with particle in the nanometric size [25].

The surface composition and chemical states of S-doped TiO_2 were measured by XPS. In Fig. 3, we present the XPS spectra of TONS-1.0 sample. It can be seen from Fig. 3a that the XPS survey spectra displays the S-doped TiO_2 contained predominantly Ti, O, C and S elements. No evidence for the corresponding peak of N element is seen, suggesting that nitrogen is not incorporated into the TONS system under our synthetic conditions.

Fig. 3b shows the XPS spectra of the S 2p region. The S 2p peak located at around 169.5 eV can be assigned to the SO_4^{2-} species [26]. It could be found that the binding energy of S 2p peaks shift slightly toward high binding energy by 0.5 eV in comparison with that of sulfur in pure SO_4^{2-} (169.0 eV). The shifting of S 2p binding energy can be ascribed to the doping of the S specie into TiO_2 lattice. Xu et al. [27] demonstrated that there are two possible coordination models between SO_4^{2-} and TiO_2 as shown in Fig. 4. It can be seen that the S^{6+} substituted for Ti^{4+} cation and eventually formed a Ti—O—S bond in the doped TiO_2 samples through the two proposed coordination models [28,29]. These results indicated that electrons partially transferred from oxygen to sulfur in sample TONS-1.0 due to the existence of Ti^{4+}. In addition, no peaks were detected around 160–163 eV in the S 2p XPS spectra, which corresponds to the Ti—S bond formed when the oxygen atoms in the TiO_2 lattice are replaced by S atoms. This suggests that the substitution of Ti^{4+} by S^{6+} is chemically more favorable than replacing O^{2-} with S^{2-} under our synthetic conditions, which is also confirmed by the previous studies of S-doped TiO_2 [28]. The formation of cationic S-doped TiO_2 could create a charge imbalance in the lattice of catalyst, and the extra positive charge is probably neutralized by the hydroxide ions.

In Fig. 3c, we show the XPS spectra of Ti 2p in S-doped TiO_2. As can be seen that the peaks centered at 459.1 and 464.9 eV due to the $2p_{3/2}$ and $2p_{1/2}$ spin–orbital splitting photoelectron, with no shifting of Ti 2p binding energy was observed, indicating the Ti element mainly existing as the chemical state of Ti^{4+}. These data are in agreement with the previously reported XPS data for S-doped TiO_2 [20]. Fig. 3d shows the O 1s XPS spectrum of TONS-1.0. The peak at 530.3 eV can be ascribed to the lattice oxygen of TiO_2, which is consistent with previous studies of TiO_2 [30].

The FT-IR spectra of S-doped TiO_2 catalysts prepared by solvothermal method with varying molar ratio of sulfur to titanium are shown in Fig. 5, which can provide the information of functional groups on the surface of materials. The spectra of FT-IR reveal that all the as-obtained TiO_2 samples including undoped sample show the same absorbance band at 1630 cm^{-1} indicative of the O—H bending vibration [31,32]. These species play a vital role in photocatalytic activity since it could act as an active oxidizer to lead to the decomposition of organic pollutants. All the samples present similar spectra that a strong absorbance band appeared in the range of 800–550 cm^{-1}, which can be attributed to the stretching vibration of Ti—O—Ti bond [16,33]. In comparison with the undoped TiO_2 catalyst, the S-doped TiO_2 samples show additional two absorbance peaks around 1135 and 1040 cm^{-1}, respectively,

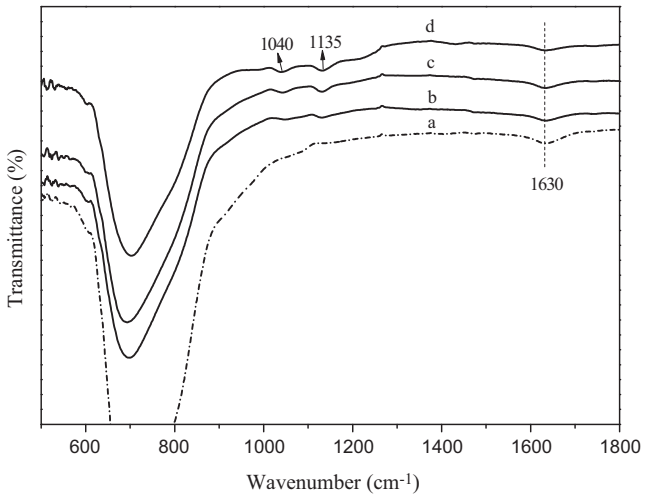

Fig. 5. FT-IR spectra of the S-doped TiO_2 samples with different starting S:Ti molar ratio. (a) undoped TiO_2, (b) TONS-0.5, (c) TONS-1.0, (d) TONS-1.5.

indicating that the formation of some new S species in TiO_2 during nonmetal doping process. Moreover, the two peaks present on the FT-IR spectra of S-doped TiO_2 suggest the presence of more than one sulfur species. The peak at 1135 cm^{-1} corresponds to the physical adsorbed SO_2, while the peak at 1040 cm^{-1} is resulted from the vibration of Ti—O—S bond [34], which clearly indicates the incorporation of S atom into the TiO_2 lattice, it therefore resulted in the narrow of the TiO_2 energy band gap and the enhancement of the visible light-induced photocatalytic performance, and is in well agreement with the XPS analysis above. In addition, the characteristic peak of Ti—O—S bonds were not observed in the undoped TiO_2.

Fig. 6 shows the representative SEM morphology of TONS-1.0 sample after being calcined at 450 °C for 3 h. It is obvious that the surface of the S-doped TiO_2 catalyst is smooth and uniform. Moreover, the TONS-1.0 sample presents large aggregates of TiO_2 nanoparticles morphology. While observation of aggregate sizes over 3 μm may not give an accurate indication of TiO_2 average size (see Fig. 6, spectrum 1 and spectrum 2 position).

Fig. 7 shows the corresponding UV–vis diffuse reflectance spectra of undoped TiO_2 and S-doped TiO_2 prepared with different molar ratios of sulfur to titanium. It was seen that the undoped

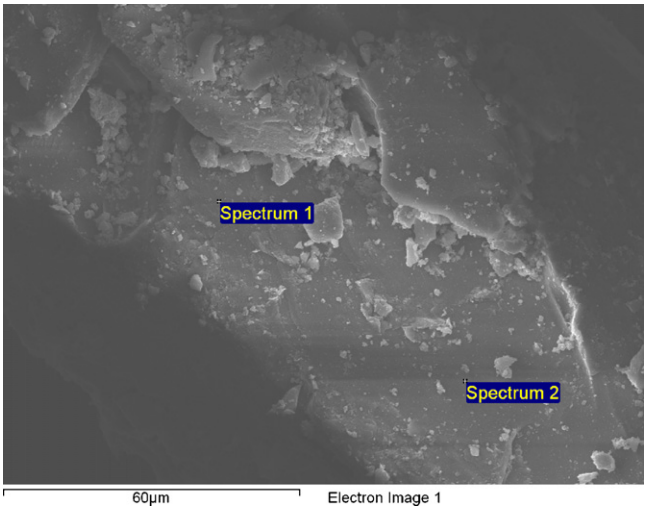

Fig. 6. SEM microphotographs of S-doped TiO_2 prepared by solvothermal method with S:Ti molar ratio of 1/1.

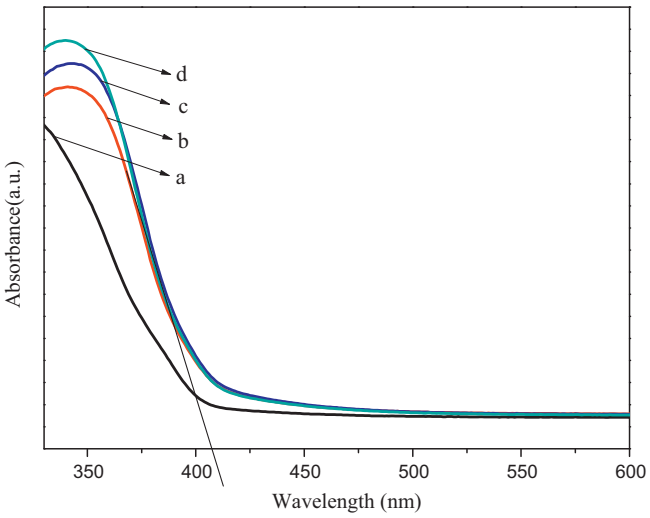

Fig. 7. UV–vis absorbance spectra of pure TiO_2 and S-doped TiO_2 (a) pure TiO_2 (P25), (b) TONS-0.5, (c) TONS-1.0, (d) TONS-1.5.

TiO_2 displays no significant absorbance in visible light region which could be easily understood by considering its wide band gap (3.2 eV). The optical absorption spectra show that all the doped samples have remarkable absorption in the visible area between 390 and 500 nm. Meanwhile, the adsorption edges of all the doped TiO_2 photocatalysts are similar, and a red-shift of about 408 nm was observed on the UV–vis DRS spectra, which corresponds to a band-gap energy of 3.04 eV. Comparison with pure commercial TiO_2 shows that S-doped TiO_2 has an obvious narrow band gap; this is just due to the doping of S species into TiO_2 lattice, thus altering its crystal and electronic structures [35], and leading to the appearance of intermediate energy level via forming Ti—O—S bond in TiO_2 and harvests visible light absorption for the doped samples.

The photocatalytic activity of S-doped TiO_2 was probed by photodegradation of Methylene Blue and phenol. A 300 W xenon lamp was used as the light source, which equipped with 420 nm cut-off glass filter to completely remove the UV light and ensures illumination by visible light only. Fig. 8 shows the corresponding adsorption curve of MB solution over the S-doped TiO_2 and pure TiO_2 in dark environment. After 30 min adsorption, the adsorption curves of the two photocatalysts become parallel, suggesting that Methylene

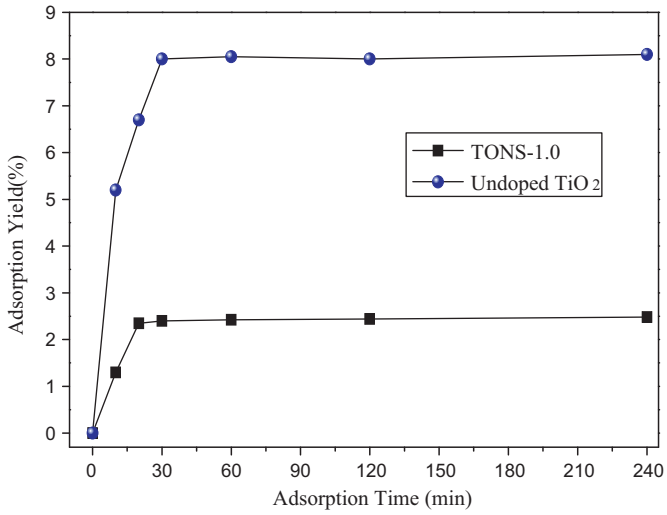

Fig. 8. MB adsorption curves on different catalysts. Adsorption conditions: 0.050 g catalyst, 50.0 mL 0.010 g/L MB, temperature = 283 K.

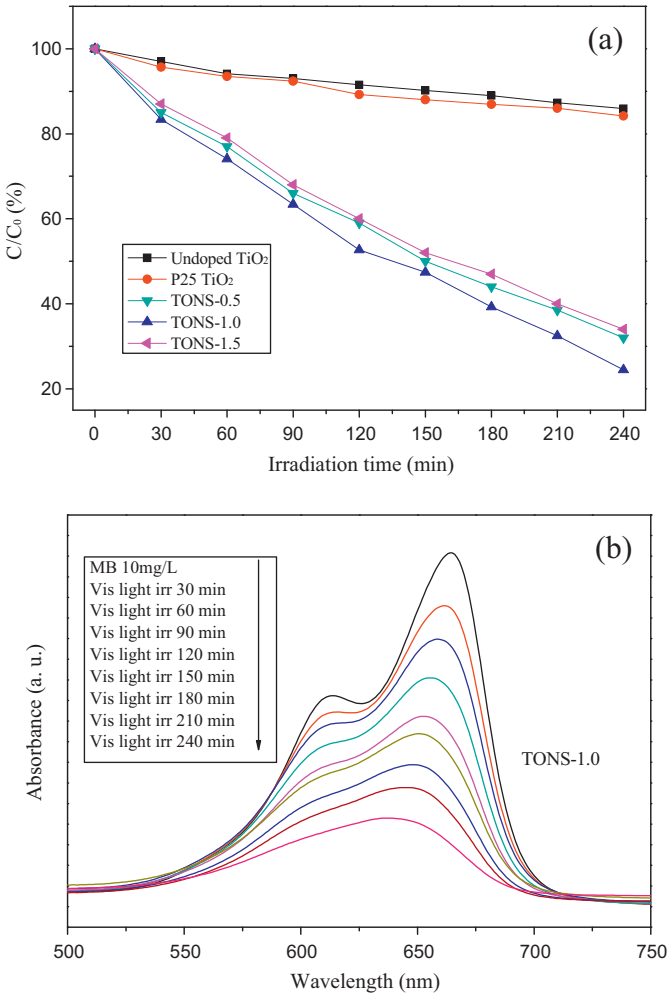

Fig. 9. (a) Photocatalytic degradation of Methylene Blue (MB) over TONS-1.0 and pure TiO_2 samples under visible light irradiation ($\lambda > 420$ nm). (b) UV––vis spectra of MB vs. photoreaction time in the presence of TONS-1.0 sample. Reaction conditions: $C_0 = 10$ ppm, catalyst loading: 1 g/L.

Blue absorption over the doped and undoped titania samples have completely reached equilibrium. Meanwhile, it also can be seen that the MB adsorption yield for TONS-1.0 sample is only 2.3% in 240 min absorption, which is much lower than that of undoped TiO_2 (the adsorption yield of MB is about 8%).

Fig. 9a shows the photocatalytic activity of the undoped TiO_2 and S-doped TiO_2 evaluated by degradation of Methylene Blue solution under visible light irradiation, and Fig. 9b shows the absorption spectra variation of MB versus irradiation time on the TONS-1.0 sample. A weak photodegradation of MB on undoped TiO_2 and P25 sample were observed as shown in Fig. 9a, which can be attributed to the dye-sensitized photocatalysis, as the pure TiO_2 has large energy band-gap, and that cannot be activated by visible light. S-doped TiO_2 showed the enhanced photocatalytic activity under visible light irradiation as compared with the references, suggesting that the S doping level had an obvious influence on the photocatalytic activity of the TiO_2 samples. TONS-1.0 shows the highest activity among the S-doped TiO_2 samples, on which about 85% MB was degraded within 240 min of visible-light irradiation. The characteristic absorption band of MB at 664 nm diminished quickly (Fig. 9b), accompanied by a slight concomitant blue-shift from 664 to 640 nm of the maximum absorption band, which indicated that MB had not only been decomposed but also mineralized in the presence of S-doped TiO_2.

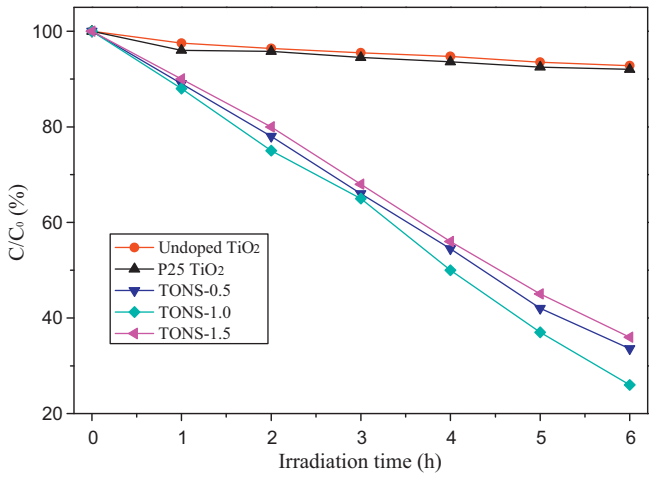

Fig. 10. Photocatalytic degradation of phenol over TiO_2 samples with varying S:TiO_2 molar ratio under visible light irradiation ($\lambda > 420$ nm). Reaction conditions: $C_0 = 10$ ppm, catalyst loading: 1 g/L.

In order to avoid the photosensitized process of MB molecules, the activity of the as-prepared catalysts was also evaluated by photocatalytic degradation of phenol under visible lights irradiation ($\lambda > 420$ nm). Fig. 10 shows the degradation of phenol over pure titania and S-doped TiO_2 with varying S doping level. It is evident that all the S-doped TiO_2 samples are more active than commercial TiO_2. After 6 h of irradiation, the values of decomposed Phenol are, respectively, 67%, 74% and 64% for TONS-0.5, TONS-1.0 and TONS-1.5 catalysts. It was seen that the TONS-1.0 sample exhibits the highest activity among all S-doped TiO_2 samples. As described above, both the degradation of Methylene Blue and phenol solution over the S-doped TiO_2 samples show similar trends: S-doping can enhance visible light activity. This observation displays that some changes have occurred in the excitation energy gap by doping with S, the doping samples becoming able to absorb light in the visible region.

In the present study, FT-IR spectra of the TONS-1.0 sample before and after the photodegradation experiments were also collected using Bruker Vertex-70 FT-IR spectrometer to examine their structure and the functional group on the surface of doped material. Fig. 11 shows the FT-IR spectra of S-doped TiO_2 before and after the photodecomposition of MB solution. No significant changes

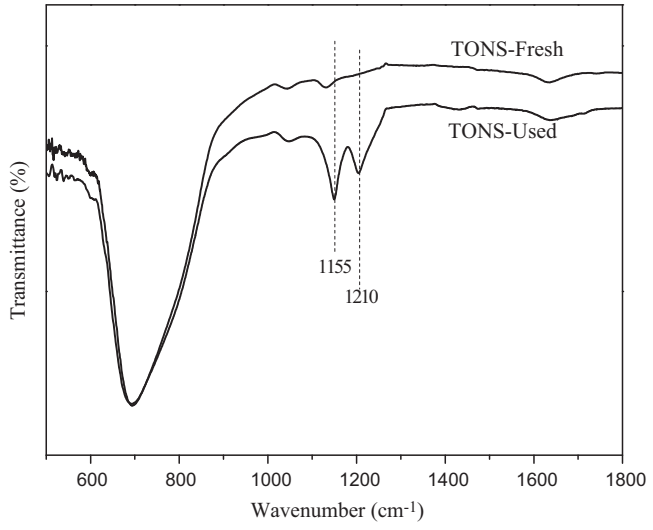

Fig. 11. FT-IR spectra of S-doped TiO_2 before and after photodegradation of Methylene Blue molecules.

have been found for the S-doped TiO_2 sample after 240 min of photocatalysis reaction, and the peaks attributed to the stretching vibration of the Ti—O—Ti bonds and the vibrations of Ti—O—S bonds are remaining existence, suggesting the TONS-1.0 sample has well crystallized anatase structure and excellent durability. Compared to the fresh photocatalyst, the FT-IR spectra of the used TiO_2 revealed that, besides the absorbance peaks from TiO_2, the TONS-1.0 sample exhibits two additional absorbance peaks, which were located at 1155 and 1210 cm^{-1}, respectively, indicating the formation of some new species on the surface of S-doped TiO_2 after the photoreaction, and it is thought that these peaks might either come from the formation of SO_2Cl_2 species during the photoreaction, or arise from the C—O—C bond that produced by the photodegradation MB experiment.

5. Discussion

The improvement in the visible light-induced photocatalytic activity of TiO_2 by doping with S element has been reported in several publications. Most of them pointed out that this improvement is mainly attributed to the stronger optical absorbance of S-doped TiO_2 system in the visible light area due to the decrease of band gap. According to XRD, XPS and FT-IR results in the present work, it can be inferred that S atom was successfully doped into the lattice of our TONS system by substituting the Ti^{4+} sites to form Ti—O—S bonds, and thus causes the generation of intermediate energy level in TiO_2, which are located above O 2p valence band, and as a consequence of narrowing the energy gaps of TiO_2 and shifting the optical absorption from UV region to visible region.

In addition, the photocatalytic performance of S-doped TiO_2 nanoparticles is also largely dependent on its crystalline structure, crystallinity, surface area, porosity, morphology and architecture. Firstly, X-ray diffraction patterns of the as-synthesized nanocrystal samples reveal that TiO_2 in the samples are well crystallized anatase structure, which might facilitate the transfer of photoelectrons from bulk to surface and thus promoting charge separation, leading to the enhanced quantum efficiency. On the other hand, the particle size of the as-synthesized samples seems to play a key role in the photodegradation of MB, because the smaller particle size, the larger specific surface area, which would provide stronger adsorption ability of the catalytic surface toward target molecules and better ability to photoexcite the electron-hole pairs in the active sites. More importantly, S doping could favor the formation of oxygen vacancies on surface of TiO_2, which has been confirmed by our previous study [36]. It was reported that the more oxygen vacancies or defects in the TiO_2 crystal might help to capture more photoelectrons and thus inhibit the recombination between the photoinduced electrons and holes. Meanwhile, the absorbed oxygen at oxygen vacancy sites was active for the formation the $O_2^{\bullet -}$ radical, this specie was considered to be responsible for the decomposition of pollutant molecules in the photoreaction experiments.

On the basis of the above discussion, we tentatively concluded that the S-doped TiO_2 powder obtained by treating the titanium precursor with thiourea under solvothermal conditions exhibited much higher photocatalytic activity than undoped TiO_2 due to the synergic effect of the pure anatase structure, small particle size, high crystallization degree of the anatase, sulfur impurity, together with oxygen vacancy [36]. Moreover, it is believed that the appearance of intermediate energy level via forming Ti—O—S bonds is a key factor accounting for the remarkable visible light activity of S-doped TiO_2.

6. Conclusions

In summary, we have demonstrated that the visible light responsible S-doped TiO_2 nanocrystal powder was successfully synthesized through a simple low-temperature solvothermal method. By tuning the starting molar ratio of sulfur to titanium, different S doping level photocatalysts were obtained. Based on the XPS and FT-IR analysis, we found that S anion can be doped into TiO_2 lattice in substitutional mode and form the Ti—O—S bonds, leading to the narrower band energy gap and enhance visible light absorption of the TiO_2 catalysts. In addition, the as-prepared samples show higher visible-light photocatalytic activity for degradation of Methylene Blue and phenol molecules, which is far superior to that of the commercial Degussa P25 TiO_2. This is probably due to the synergetic effect of the high crystallinity, smaller particle size, pure anatase structure, oxygen vacancies and stronger visible light absorption.

Acknowledgement

Thanks to the UK Photocatalysis Network for their kind support.

References

[1] A. Fujishima, X. Zhang, D.A. Tryk, Surf. Sci. Rep. 63 (2008) 515–582.
[2] Q. Zhang, C.S. Dandeneau, X. Zhou, G. Cao, Adv. Mater. 21 (2009) 4087–4108.
[3] H. Zhang, G. Chen, D.W. Bahnemann, J. Mater. Chem. 19 (2009) 5089–5121.
[4] T. Ohno, M. Akiyoshi, T. Umebayashi, K. Asai, T. Mitsui, M. Matsumura, Appl. Catal. A 265 (2004) 115–121.
[5] T. Morikawa, T. Ohwaki, K. Suzuki, S. Moribe, S. Tero-Kubota, Appl. Catal. B 83 (2008) 56–62.
[6] F. Han, V.S.R. Kambala, M. Srinivasan, D. Rajarathnam, R. Naidu, Appl. Catal. A 359 (2009) 25–40.
[7] J. Ye, W. Liu, J. Cai, S. Chen, X. Zhao, H. Zhou, L. Qi, J. Am. Chem. Soc. 133 (2011) 933–940.
[8] D.V. Talapin, J.-S. Lee, M.V. Kovalenko, E.V. Shevchenko, Chem. Rev. 110 (2010) 389.
[9] A. Kudo, K. Omori, H. Kato, J. Am. Chem. Soc. 121 (1999) 11459.
[10] Z. He, Y. Li, Q. Zhang, H. Wang, Appl. Catal. B 93 (2010) 376–382.
[11] U.G. Akpan, B.H. Hameed, Appl. Catal. A 375 (2010) 1–11.
[12] L.M. Petkovic, D.M. Ginosar, H.W. Rollins, K.C. Burch, P.J. Pinhero, H.H. Farrell, Appl. Catal. A 338 (2008) 27–36.
[13] Y.Z. Yang, C.-H. Chang, H. Idriss, Appl. Catal. B 67 (2006) 217–222.
[14] H. Uchiyama, H. Imai, Chem. Commun. (2005) 6014–6016.
[15] S.C. Hayden, N.K. Allam, M.A. Ei-Sayed, J. Am. Chem. Soc. 132 (2010) 14406–14408.
[16] G. Yang, Z. Jiang, H. Shi, T. Xiao, Z. Yan, J. Mater. Chem. 20 (2010) 5301–5309.
[17] J.K. Zhou, L. Lv, J. Yu, H.L. Li, P.-Z. Guo, H. Sun, X.S. Zhao, J. Phys. Chem. C 112 (2008) 5316–5321.
[18] X. Yang, C. Cao, K. Hohn, L. Erickson, R. Maghirang, D. Hamal, K. Klabunde, J. Catal. 252 (2007) 296–302.
[19] X. Chen, C. Burda, J. Am. Chem. Soc. 130 (2008) 5018–5019.
[20] H. Li, X. Zhang, Y. Huo, J. Zhu, Environ. Sci. Technol. 41 (2007) 4410–4414.
[21] K. Yanagisawa, J. Ovenstone, J. Phys. Chem. B 103 (1999) 7781–7787.
[22] K.L. Frindell, M.H. Bartl, A. Popitsch, G.D. Stucky, Angew. Chem. Int. Ed. 41 (2002) 959–962.
[23] W. Ma, Z. Lu, M. Zhang, Appl. Phys. A 66 (1998) 621.
[24] J. Parker, R. Siegel, J. Mater. Res. 5 (1990) 1246.
[25] M.M. Oliveria, D.C. Schnizler, A.J.C. Zarbin, Chem. Mater. 15 (2003) 1903–1909.
[26] F. Wei, L. Ni, P. Cui, J. Hazard. Mater. 156 (2008) 135–140.
[27] J.-H. Xu, J. Li, W.-L. Dai, Y. Cao, H. Li, K. Fan, Appl. Catal. B 79 (2008) 72–80.
[28] J.C. Yu, W.K. Ho, J.G. Yu, H. Yip, P.K. Wong, J.C. Zhao, Environ. Sci. Technol. 39 (2005) 1175.
[29] F. Dong, W. Zhao, Z. Wu, Nanotechnology 19 (2008) 365607.
[30] J. Wang, W. Zhu, Y. Zhang, S. Liu, J. Phys. Chem. C 111 (2007) 1010.
[31] Y. Huo, Y.Jin, J. Zhu, H. Li, Appl. Catal. B 89 (2009) 543–550.
[32] K.L. Yeung, S.T. Yau, A.J. Maira, J.M. Coronado, J. Soria, P.L. Yue, J. Catal. 219 (2003) 107.
[33] D. Huang, S. Liao, S. Quan, L. Liu, Z. He, J. Wan, W. Zhou, J. Mater. Res. 22 (2007) 2389–2397.
[34] G. Yang, T. Xiao, J. Sloan, G. Li, Z. Yan, Chem. Eur. J. 17 (2011) 1096–1100.
[35] W. Ho, J.C. Yu, S. Lee, J. Solid State Chem. 179 (2006) 1171–1176.
[36] G. Yang, Z. Jiang, H. Shi, M.O. Jones, T. Xiao, P.P. Edwards, Z. Yan, Appl. Catal. B 96 (2010) 458–465.